Using PS-InSAR observations to detect aseismic fault slip in the seismically active Groningen gas field

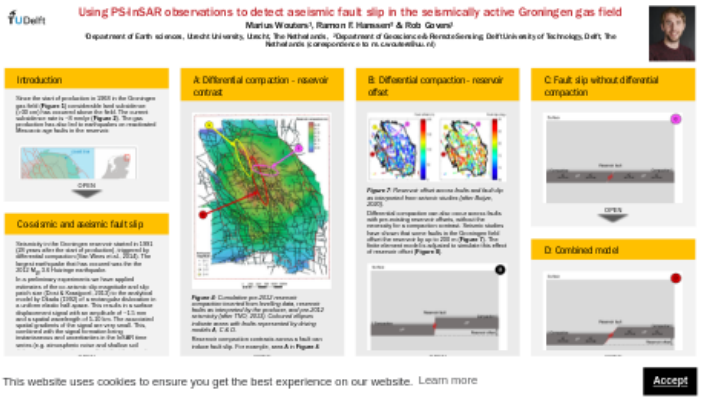

Marius Wouters[1], Ramon F. Hanssen[2] & Rob Govers[1]

[1]Department of Earth sciences, Utrecht University, Utrecht, The Netherlands, [2]Department of Geoscience & Remote Sensing, Delft University of Technology, Delft, The Netherlands (correspondence to: m.c.wouters@uu.nl)

PRESENTED AT:

INTRODUCTION

Since the start of production in 1968 in the Groningen gas field (**Figure 1**) considerable land subsidence (>30 cm) has occurred above the field. The current subsidence rate is ~8 mm/yr (**Figure 2**). The gas production has also led to earthquakes on reactivated Mesozoic age faults in the reservoir.

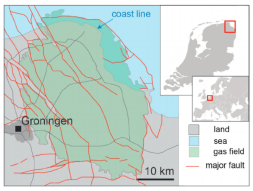

***Figure 1**: Map of the Groningen gas field area (NE Netherlands), next to the city of Groningen. Major reservoir faults are also shown (after Pijnenburg et al., 2018).*

This study is part of the DeepNL/Subsidence project, which aims to identify the subsurface drivers for the subsidence above the gas field, by assimilating geodetic time series (e.g. InSAR; **Figure 2**) into geophysical subsurface models. In order to build an efficient model for the reservoir and overburden, we model only those features that produce a detectable surface signal. Thus we investigate: **does reservoir fault slip produce surface signals that are detectable in the geodetic time series?**

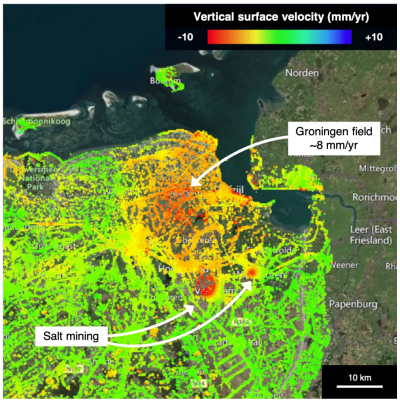

***Figure 2**: InSAR derived vertical surface displacement rate (source: bodemdalingskaart.nl (http://bodemdalingskaart.nl)). Areas of shallow salt mining are ignored in this study.*

CO-SEISMIC AND ASEISMIC FAULT SLIP

Seismicity in the Groningen reservoir started in 1991 (28 years after the start of production), triggered by differential compaction (Van Wees et al., 2014). The largest earthquake that has occured was the the 2012 M_W 3.6 Huizinge earthquake.

In a preliminary experiments we have applied estimates of the co-seismic slip magnitude and slip patch size (Dost & Kraaijpoel, 2013) to the analytical model by Okada (1992) of a rectangular dislocation in a uniform elastic half-space. This results in a surface displacement signal with an amplitude of ~1.5 mm and a spatial wavelength of 5-10 km. The associated spatial gradients of the signal are very small. This, combined with the signal formation being instantaneous and uncertianties in the InSAR time series (e.g. atmospheric noise and shallow soil deformation), makes it very unlikely that the signal is detectable. The co-seismic signal of lower magnitude earthquakes will be even smaller.

However, fault slip can also occur without producing earthquakes: aseismic slip (creeping faults). Here we investigate the surface displacement footprint of potential aseismic fault slip, for three different driving mechanisms (A-C) and a combined model (D).

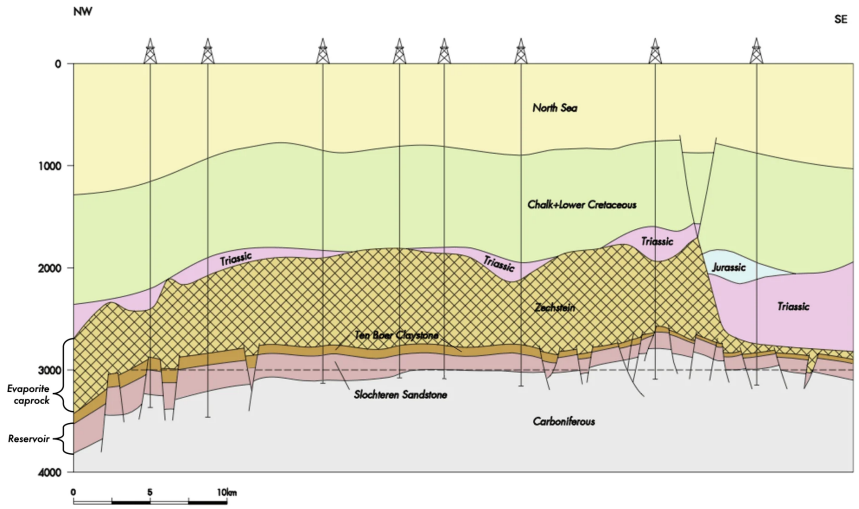

Figure 3*: Cross-section through the Groningen gas field area. Seismicity occurs on the faults cutting the Slochteren Sandstone reservoir.*

A: DIFFERENTIAL COMPACTION - RESERVOIR CONTRAST

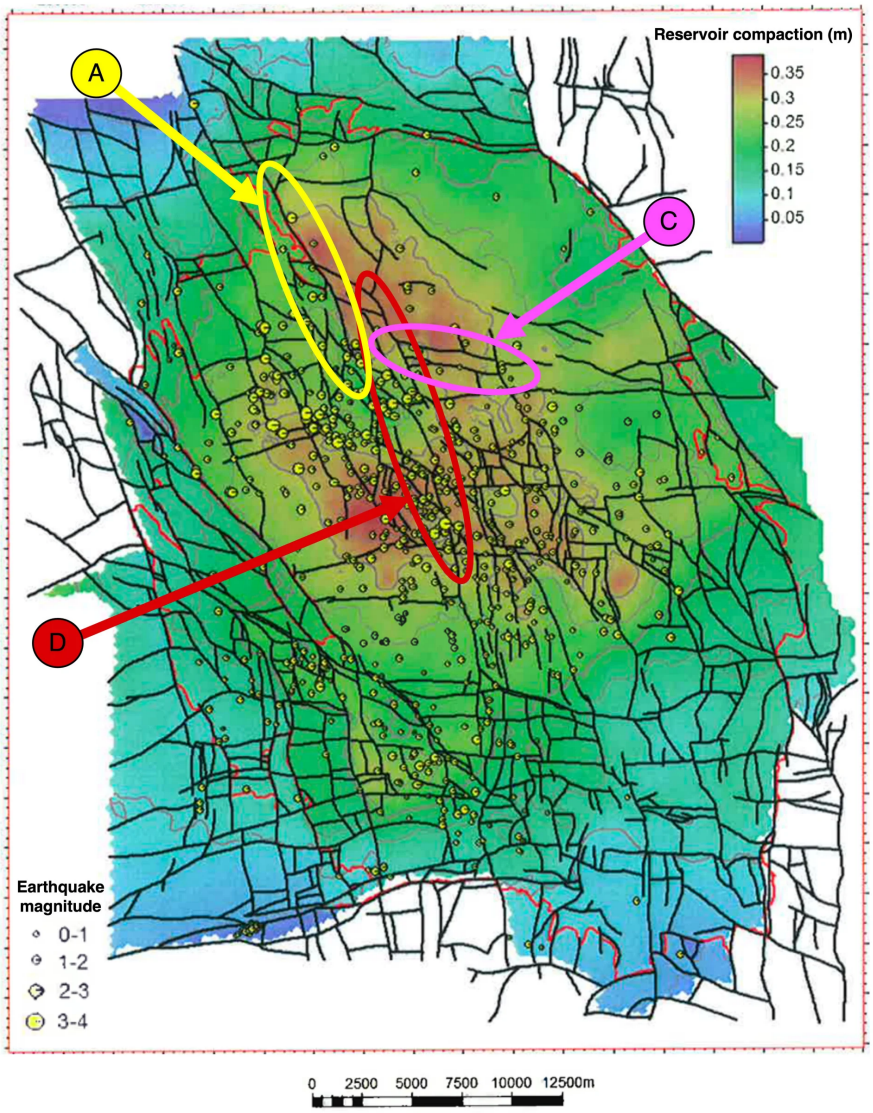

***Figure 4**: Cumulative pre-2012 reservoir compaction inverted from levelling data, reservoir faults as interpreted by the producer, and pre-2012 seismicity (after TNO, 2013). Coloured ellipses indicate areas with faults represented by driving models A, C & D.*

Reservoir compaction contrasts across a fault can induce fault slip. For example, area A in **Figure 4** shows a large fault with a significant compaction constrast.

To simulate to potential aseismic fault slip for such differential compaction, we use a 2D plane strain finite element model (GTECTON; Govers & Meijer, 2001) of a vertical fault seperating two reservoir sections, of which only one is compacting (**Figure 5**). Compaction is driven by a 0.36 MPa/yr pressure change (ΔP), representing the approximate yearly field-average pore pressure drop.

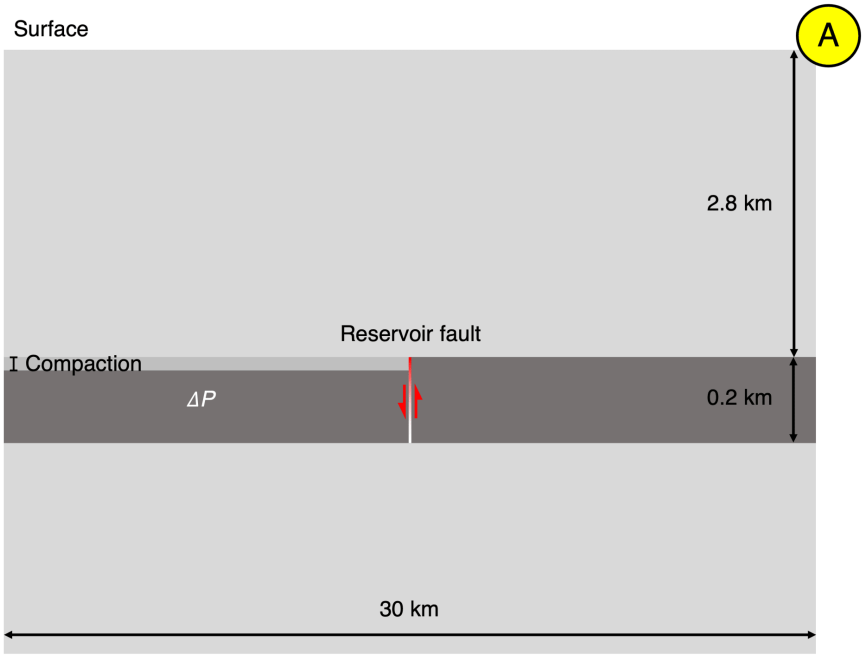

***Figure 5**: Schematic diagram of the finite element model setup simulating driving mechanism A. Dark grey layer is the reservoir, with only the left half compacting. Material properties are uniform.*

We run two version of the model: one with the fault locked (no aseismic slip) and one with an unlocked frictionless fault (continuous aseismic slip). With an applied yearly pressure drop, the surface modelled surface deformation represent the surface displacement rate (**Figure 6a**). In order to visualise the difference between the results of the two model versions, **Figure 6b** shows the residual. This residual represents the impact of aseismic fault slip.

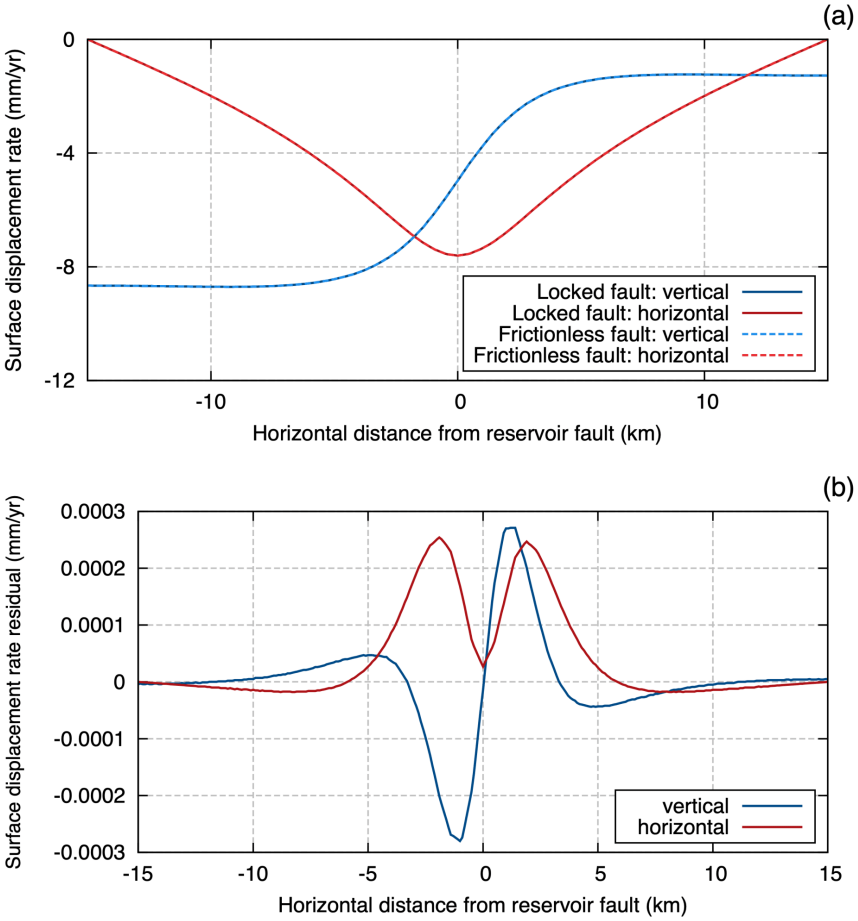

***Figure 6**: (a) Surface displacement rates of both locked and unlocked version of the model of **Figure 5**. Note that on the scale of the full signal, the signals look identical, hence the overlap. (b) The difference between the results of the two versions.*

The results of **Figure 6** show that the impact of the aseismic fault slip is tiny (more than four orders of magnitude smaller than the overall surface signal of **Figure 2**). This is caused by the compacting reservoir section being subject to strong elastic support (stress arching) from the not-compacting section.

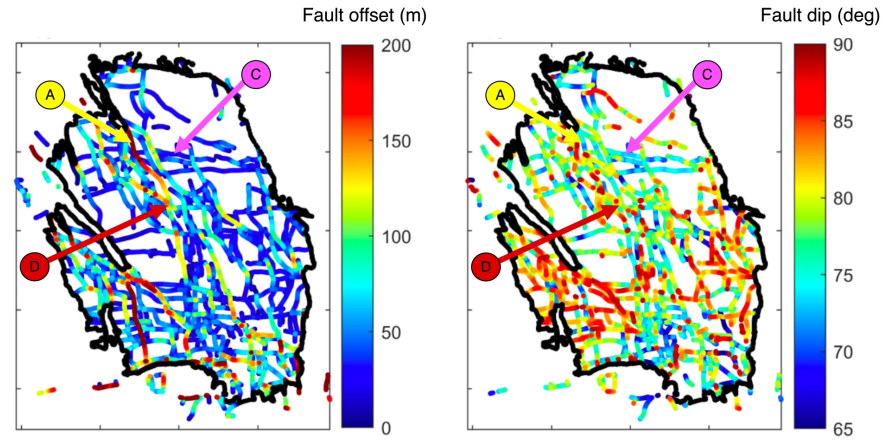

***Figure 7**: Reservoir offset across faults and fault dip as interpreted from seismic studies (after Buijze, 2020).*

Differential compaction can also occur across faults with pre-existing reservoir offsets, without the necessity for a compaction contrast. Seismic studies have shown that some faults in the Groningen field offset the reservoir by up to 200 m (**Figure 7**). The finite element model is adjusted to simulate this effect of reservoir offset (**Figure 8**).

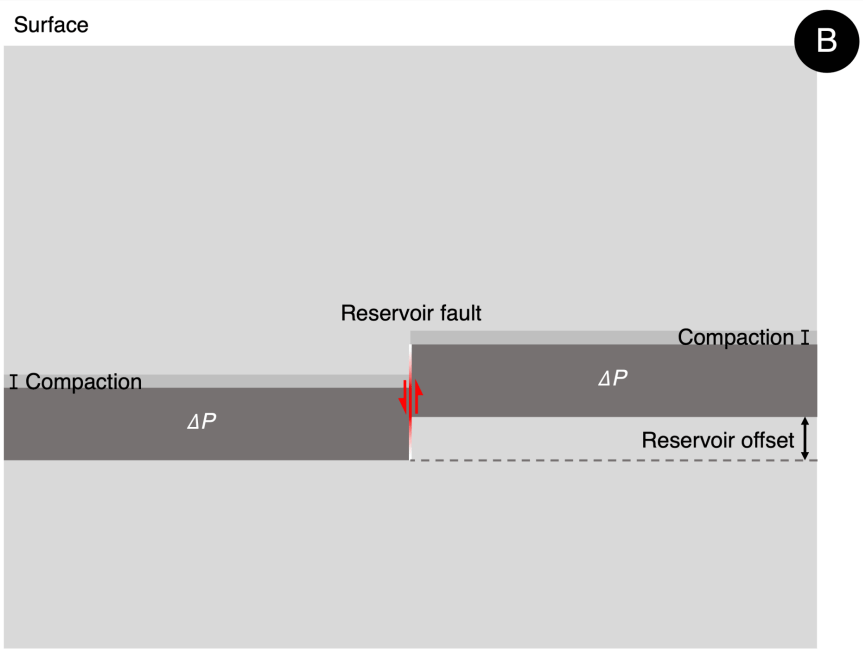

***Figure 8**: Schematic diagram of the finite element model setup simulating driving mechanism B.*

The surface displacement result of this setup is shown in **Figure 9**.

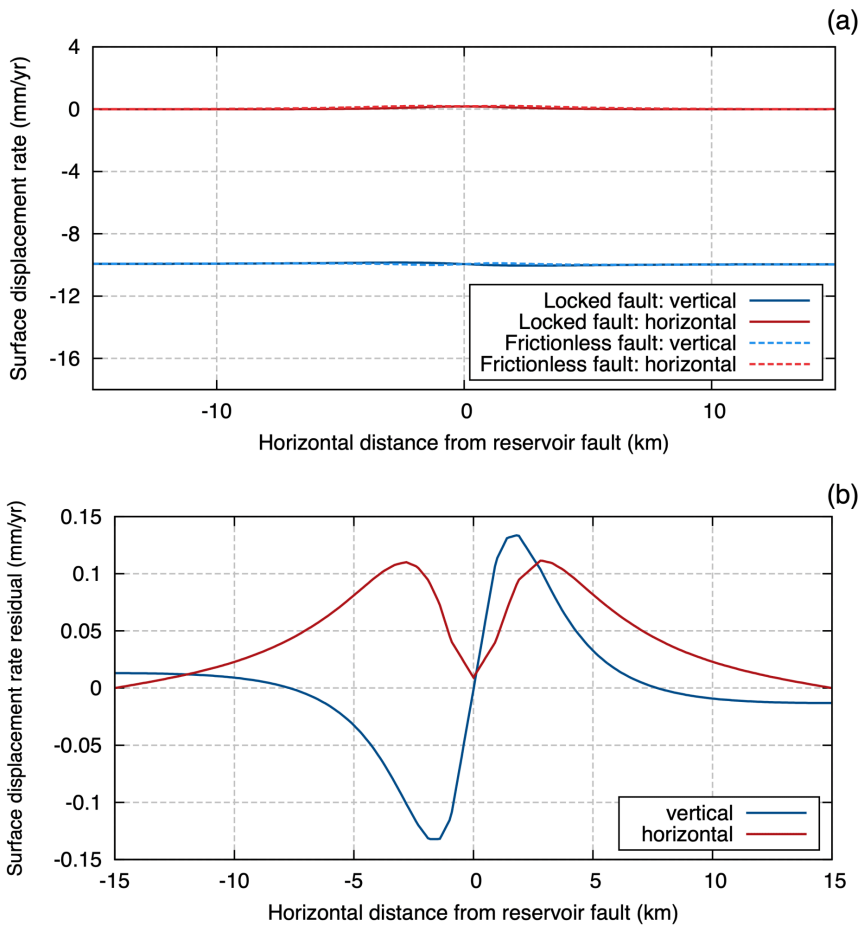

***Figure 9**: As **Figure 6**, but for the model setup of **Figure 8**. Reservoir offset used is 150 m.*

The residual signal amplitude increases as the reservoir offset gets larger (**Figure 10**). However, the signal is still over an order of magntitude smaller than the overall signal of **Figure 2**.

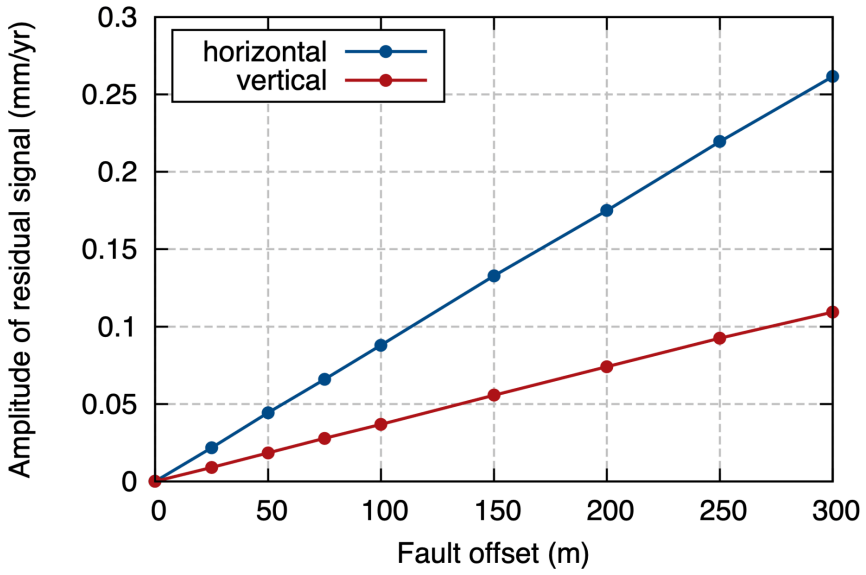

***Figure 10**: Relationship between the applied reservoir offset and amplitude of the residual surface displacement rate signal.*

C: FAULT SLIP WITHOUT DIFFERENTIAL COMPACTION

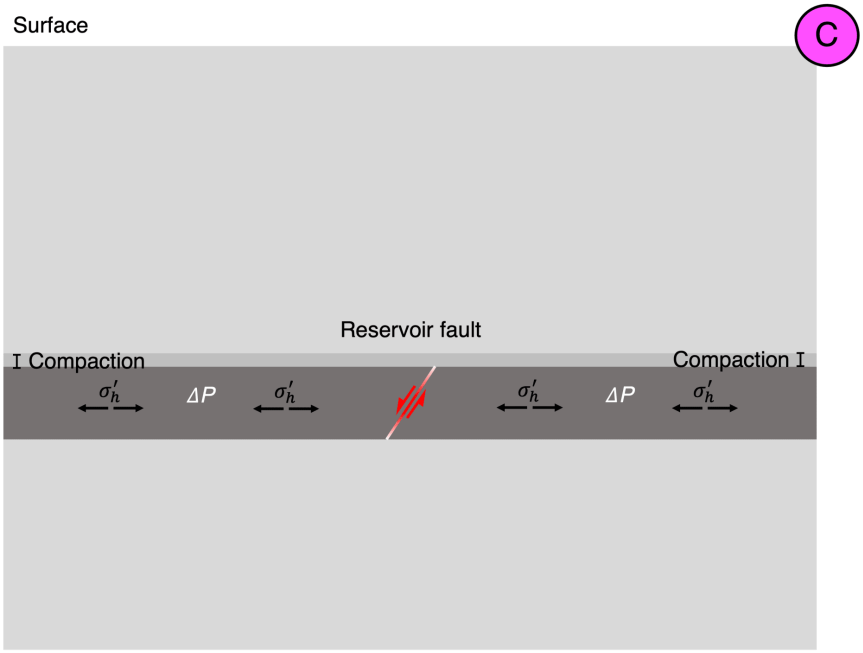

***Figure 11**: Schematic diagram of the finite element model setup simulating driving mechanism C. The σ'_h symbol indicates the horizontal tensional effective stresses in the reservoir.*

Reservoir fault slip can also be induced without differential compaction. Gas production causes a pore pressure reduction and vertical contraction (compaction) of the reservoir. The reservoir also wants to contract horizontally, leading to horizontal tensional (effective) stresses (e.g. Zoback & Zinke, 2002; Van Wees et al., 2014).

We isolate the effect of these horizontal stresses, using a model without any differential compaction (no offsets or compaction contrest), but with a non-vertical fault (**Figure 11**). An example area for this driving mechanims (C) is indicated on **Figures 4** and **7**. In this area the compaction is relatively strong, and compaction contrasts and reservoir offsets are small (as the geometry of **Figure 11**).

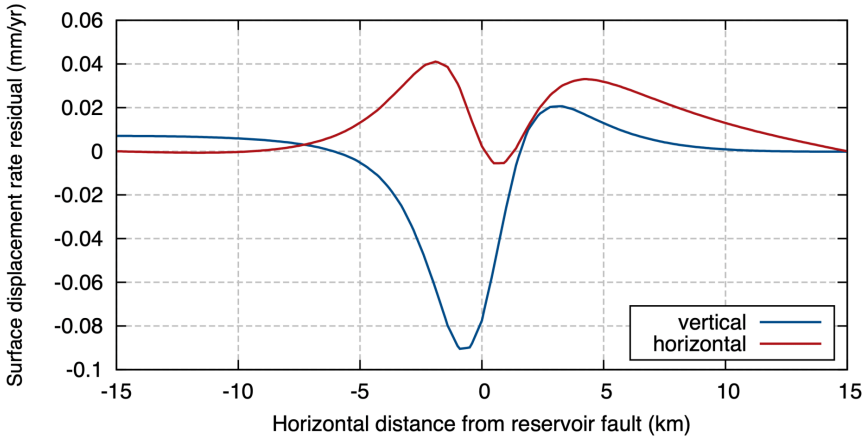

***Figure 12**: Difference between surface displacement rate results of the locked and unlocked versions of the model of **Figure 11**. A fault dip of 65°* is applied.

The magnitude of the surface signal caused by aseismic fault slip due to the horizontal stresses (**Figure 12**) is smaller than that caused by reservoir offset of driving mechanism B (**Figure 9b**). The surface signal amplitude increases as the fault dips shallower (**Figure 13**).

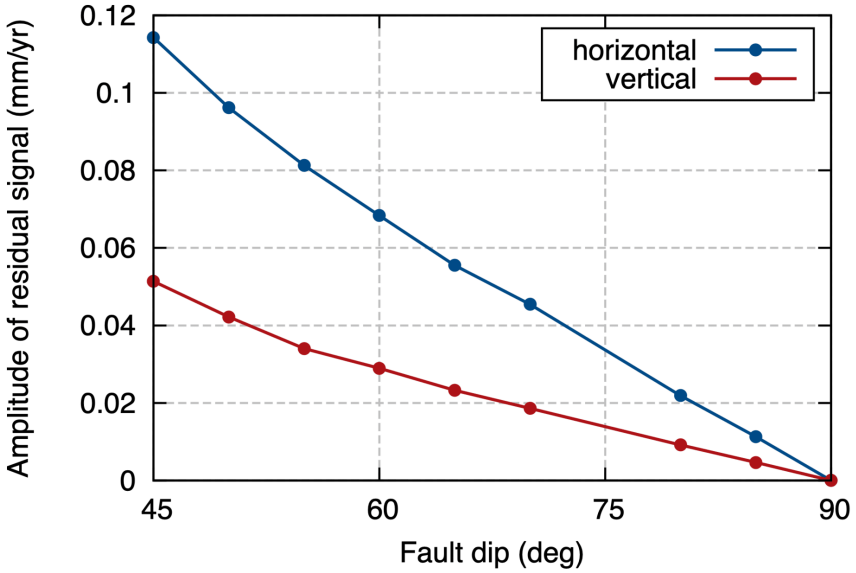

***Figure 13**: Relationship between the fault dip and amplitude of the residual surface displacment rate signal.*

D: COMBINED MODEL

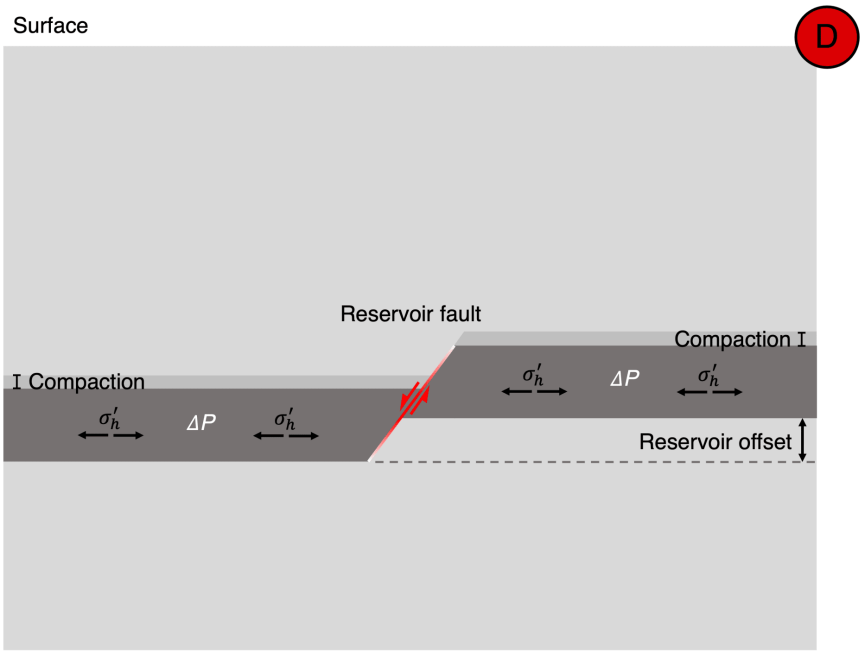

***Figure 14**: Schematic diagram of the finite element model setup simulating driving mechanism D.*

We combine the models B and C to simulate the effect of differential compaction from reservoir offset and the horizontal tensional stresses together (**Figure 14**). Such faults could be present in area D in **Figures 4** and **7**, where reservoir compaction and fault offsets are relatively large.

The resulting surface displacement residuals are shown in **Figure 15**. The combined residual amplitude is larger than that of driving mechanism B and C individually: 0.23 versus 0.13 and 0.06 mm/yr, for the vertical component.

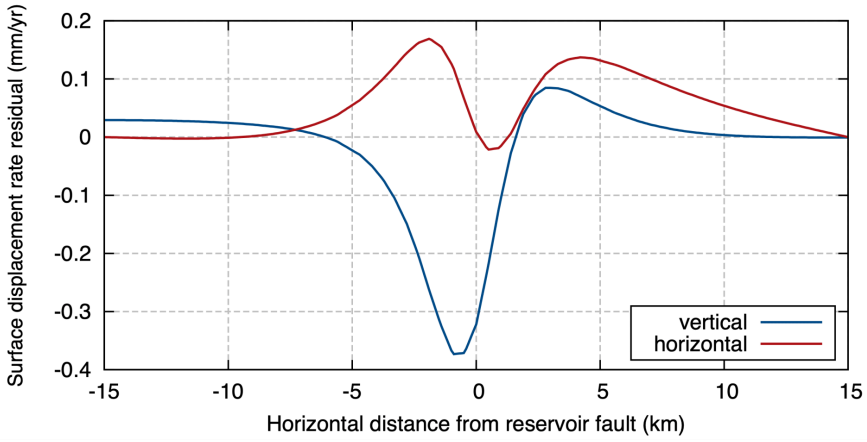

***Figure 15**: Difference between surface displacement rate results of the locked and unlocked versions of the model of **Figure 14**. Applied fault dip is 65°, fault offset is 150 m.*

Conclusions

- Aseismic fault slip due to differential compaction caused reservoir offset (B) induces the strongest surface displacement signal.
- Even with the combined effect of reservoir offset and fault dip (D), the footprint of the aseismic slip (0.23 mm/yr) is small compared to the ~8 mm/yr overall subsidence signal over the Groningen field.
- Because of the low signal amplitude, long spatial wavelength (leading to small spatial gradients), and uncertianties in the InSAR time series (e.g. atmospheric noise and shallow soil deformation), we see detecting the tiny potential aseismic slip signal within the overall signal as impossible.
- For the design of the geophysical models of the reservoir and overburden, reservoir fault slip can be ignored.

DISCLOSURES

This work is part of the project of the research programme DeepNL (NWO DEEP.NL.2018.052) which is financed by the Dutch Research Council (NWO).

ABSTRACT

Since the start of production in 1968 in the Groningen gas field (Netherlands) considerable land subsidence (>30 cm) has occurred above the field. Variability in reservoir compaction has led to earthquakes on reactivated Mesozoic age reservoir faults. Even though the impact of this seismicity ($M_W \leq 3.6$) on society has been large, due to substantial structural damage to buildings, surface deformation induced by the co-seismic slip has been too small to detect using geodetic data. It is possible that differential compaction across faults is not only accommodated by seismic slip, but also by aseismic slip (e.g., creep). Aseismically slipping reservoir faults would relax the stresses in the reservoir and, thus, reduce the severity of the seismicity. In this study we explore the potential occurrence of aseismic slip on the reservoir faults.

We perform a sensitivity analysis to investigate whether aseismic slip on the different reservoir faults has the capacity to produce detectable surface signals. We use the analytical Okada (1992) model of slip on a discrete dislocation in a uniform elastic half-space to simulate the deformations originating from slip on a wide range of fault geometries, representing the variability in the field. Unsurprisingly, laterally extensive faults with strong compaction contrasts across them (large differential slip magnitudes) produce the largest surface signals. To determine which potentially aseismically slipping faults produce surface signals that could be detectable in persistent scatterer InSAR time series, we analyze the surface patterns for large differential displacements across large length scales, since InSAR observations are most sensitive to spatially extensive patterns with high spatial gradients.

We use the results of the sensitivity analysis to guide our search for patterns originating from aseismically slipping reservoir faults in PS-InSAR time series data of the Groningen area. First results show that these specific patterns are rare, indicating that the amount of aseismic slip is limited. For faults lacking surface signals related aseismic slip, the results of sensitivity analysis are used to determine upper limits for the aseismic differential slip magnitudes.

REFERENCES

Buijze, A. J. L. (2020). Numerical and experimental simulation of fault reactivation and earthquake rupture applied to induced seismicity in the Groningen gas field (Doctoral dissertation, Utrecht University). doi: 10.33540/60 (https://doi.org/10.33540/60)

Dost, B., & Kraaijpoel, D. (2013). The August 16, 2012 earthquake near Huizinge (Groningen). KNMI Scientific Report. Royal Netherlands Meteorological Institute (KNMI), Utrecht, The Netherlands. source: nam.nl (https://www.nam.nl/shared/politics-and-governance/_jcr_content/par/textimage.stream/1453326117407/1f98cbd2cd7c69773c697008676e756deeaac61a/the-august-16-2012-earthquake-near-huizinge-groningen1.pdf)

Govers, R., & Meijer, P. T. (2001). On the dynamics of the Juan de Fuca plate. Earth and Planetary Science Letters, 189, 115–131. doi: 10.1016/S0012-821X(01)00360-0 (https://doi.org/10.1016/S0012-821X(01)00360-0)

Okada, Y. (1992). Internal deformation due to shear and tensile faults in a half-space. Bulletin of the seismological society of America, 82(2), 1018-1040. doi: 10.1785/BSSA0820021018 (https://doi.org/10.1785/BSSA0820021018)

Pijnenburg, R. P. J., Verberne, B. A., Hangx, S. J. T., & Spiers, C. J. (2018). Deformation behavior of sandstones from the seismogenic Groningen gas field: Role of inelastic versus elastic mechanisms. Journal of Geophysical Research: Solid Earth, 123(7), 5532-5558. doi: 10.1029/2018JB015673 (https://doi.org/10.1029/2018JB015673)

TNO. (2013). Toetsing van de bodemdalingsprognoses en seismische hazard ten gevolge van gaswinning van het Groningen veld. source: tweedekamer.nl (https://www.tweedekamer.nl/downloads/document?id=9ab9da2b-299b-4e86-8ca8-7bbf751687b7&title=Toetsing%20van%20de%20bodemdalingsprognoses%20en%20seismische%20hazard%20ten%20gevolge%20van%20gaswinning%20van%20het%2

Van Wees, J. D., Buijze, L., Van Thienen-Visser, K., Nepveu, M., Wassing, B. B. T., Orlic, B., & Fokker, P. A. (2014). Geomechanics response and induced seismicity during gas field depletion in the Netherlands. Geothermics, 52, 206-219. doi: 10.1016/j.geothermics.2014.05.004 (https://doi.org/10.1016/j.geothermics.2014.05.004)

Zoback M.D., Zinke J.C. (2002) Production-induced Normal Faulting in the Valhall and Ekofisk Oil Fields. In: Trifu C.I. (eds) The Mechanism of Induced Seismicity. Pageoph Topical Volumes. Birkhäuser, Basel. doi: 10.1007/978-3-0348-8179-1_17 (https://doi.org/10.1007/978-3-0348-8179-1_17)